Metal–Insulator–Semiconductor Transmission Lines

Dylan F. Williams, *Senior Member, IEEE*

***Abstract*— This paper investigates the one-dimensional metal–insulator–semiconductor transmission line. It develops closed-form expressions for equivalent-circuit parameters, compares them to exact calculations, and explores their limitations. It also investigates the usual assumption of single-mode propagation and shows that, in certain fairly common circumstances, the fundamental mode of propagation becomes so lossy that it can no longer be considered to be the dominant propagating mode.**

***Index Terms*— Equivalent circuit, metal–insulator–semiconductor transmission line, microstrip, silicon.**

I. Introduction

THIS PAPER investigates the transverse magnetic (TM) modes of the one-dimensional metal–insulator–semiconductor (MIS) transmission line of Fig. 1. The transmission line consists of a metal film bounded on its upper surface by a perfect magnetic wall and separated by an insulator or a depletion region from a semiconducting substrate backed with a perfectly conducting wall. While this transmission line has no fringing fields, it approximates wide microstrip lines fabricated on silicon substrates backed by thick metal films of high conductivity. Here, the magnetic wall approximates the nearly open-circuit condition at the air–metal interface on top of the signal line, while the electric wall approximates the boundary condition due to the highly conductive metal film on the back of the substrate. Its solutions, when reflected through the magnetic wall, also correspond to those of the even modes of symmetric infinitely wide metal–semiconductor–insulator–metal–insulator–semiconductor–metal striplines.

Guckel *et al.* [1], Hasegawa *et al.* [2], and Jäger [3] first investigated the one-dimensional MIS transmission line. Guckel *et al.* observed that when the substrate conductivity σ_s is greater than a specific conductivity σ_{min}, the MIS line will be dominated by series loss, and that when σ_s is less than σ_{min}, the MIS line will be dominated by shunt loss. They used σ_{min} to define two distinct regions of operation. They treated these two regions of operation independently and developed different equivalent-circuit descriptions for each of them.

Hasegawa *et al.* carried these concepts further in [2]. This work discussed three MIS regions of operation, each separated from the others by a transition region and described by its own distinct equivalent-circuit model.

In [3], Jäger focused on what he called the "slow wave" region of propagation of the MIS line. Jäger deviated significantly from the treatments of [1] and [2] by proposing an equivalent-circuit model in which the resistance of the substrate is connected in parallel with the resistances of the metal and insulator, rather than in series with them.

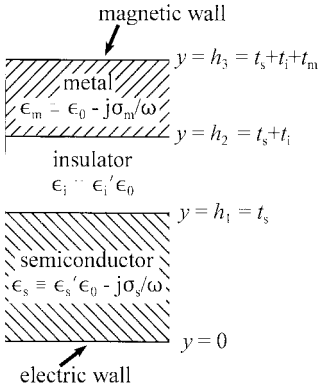

Fig. 1. The one-dimensional MIS transmission line.

These three investigations of the one-dimensional MIS lines have played a crucial role in shaping our understanding of the broader class of MIS transmission lines; almost all subsequent investigations of more complex MIS lines with fringing fields have focused on extensions of the basic circuit models they described.

This paper will report on single unified equivalent-circuit descriptions for the dominant TM_0 mode of the one-dimensional MIS line valid over all its regions of operation. It will also present the first application of the integral expressions of [4] and [5] for a transmission line's equivalent-circuit parameters to the development of a closed-form equivalent-circuit model for a transmission line. Finally, this paper will investigate the common assumption that the TM_0 mode of the MIS line is always dominant and examine its properties when it becomes so lossy that it can no longer be considered dominant.

II. Exact Modal Solutions

It is customary to refer to the nth TM mode of a transmission line, where n refers to the order of the mode, as the TM_n mode. When the transmission line is lossless, n refers to the number of nulls in TM field, and higher values of n correspond to higher spatial variation in the transverse fields. When the transmission line is lossy, the modes are ordered so that the transverse variation in the transverse fields increases with increasing n.

Reference [6] outlines a method of solving exactly for the propagation constant and fields of any TM_n mode of the one-dimensional transmission line of Fig. 1. Define the complex

Manuscript received February 25, 1998.

The author is with the National Institute of Standards and Technology, Boulder, CO 80303 USA (e-mail: dylan@boulder.nist.gov).

Publisher Item Identifier S 0018-9480(99)01152-7.

dielectric constant $\epsilon_{\rm m}$ of the metal to be $\epsilon_0 - j\sigma_{\rm m}/\omega$, where ϵ_0 is the permittivity of free space, $\sigma_{\rm m}$ is the conductivity of the metal, and ω is the angular frequency, the dielectric constant $\epsilon_{\rm i}$ of the insulator to be $\epsilon'_{\rm i}\epsilon_0$, where $\epsilon'_{\rm i}$ is the relative dielectric constant of the insulator, and the complex dielectric constant $\epsilon_{\rm s}$ of the semiconductor to be $\epsilon'_{\rm s}\epsilon_0 - j\sigma_{\rm s}/\omega$, where $\epsilon'_{\rm s}$ is its relative dielectric constant and $\sigma_{\rm s}$ is its conductivity. Then the longitudinal electric field of a TM mode of propagation in the MIS line of Fig. 1 can be written as [6]

$$E_z = \begin{cases} \cos(k_{\rm m}(h_3 - y), & h_3 \geq y \geq h_2 \\ B\,\sin(k_{\rm i}(h_2 - y)) + C\,\cos(k_{\rm i}(h_2 - y), & h_2 \geq y \geq h_1 \\ D\,\sin(k_{\rm s} y), & h_1 \geq y \geq 0 \end{cases} \tag{1}$$

and its tangential magnetic field as

$$H_x = \begin{cases} \dfrac{j\omega\epsilon_{\rm m}}{k_{\rm m}}\,\sin(k_{\rm m}(h_3 - y)), & h_3 \geq y \geq h_2 \\ \dfrac{j\omega\epsilon_{\rm i}}{k_{\rm i}}\,[-B\,\cos(k_{\rm i}(h_2 - y)) + C\,\sin(k_{\rm i}(h_2 - y)], & h_2 \geq y \geq h_1 \\ \dfrac{j\omega\epsilon_{\rm s}}{k_{\rm s}}\,D\,\cos(k_{\rm s} y), & h_1 \geq y \geq 0. \end{cases} \tag{2}$$

Here, $h_1 \equiv t_{\rm s}$, $h_2 \equiv t_{\rm i} + t_{\rm s}$, and $h_3 \equiv t_{\rm m} + t_{\rm i} + t_{\rm s}$, where $t_{\rm m}$, $t_{\rm i}$, and $t_{\rm s}$ are the thicknesses of the metal, insulator, and semiconducting substrate. In addition, $H_z = H_y = E_x = 0$, the fields have been normalized so that $E_z = 1$ at $y = h_3$; the implicit dependence $e^{+j\omega t}e^{-\gamma z}$, where γ is the modal propagation constant, has been suppressed throughout, and the mode's tangential electric field E_y is

$$E_y = -\frac{\gamma}{j\omega\epsilon_\tau}\,H_x. \tag{3}$$

The constants $k_{\rm m}$, $k_{\rm i}$, and $k_{\rm s}$ are defined by

$$k_\tau^2 \equiv \gamma^2 + \omega^2\epsilon_\tau\mu_0 \tag{4}$$

where τ takes the values m, i, or s as appropriate, and μ_0 is the permeability of free space. The k_τ describe the variation of the fields in the y-direction and are usually complex. At low frequencies, $k_{\rm m}$ is small and the currents in the metal are nearly uniform. For good conductors at high frequencies, $k_{\rm m}$ approaches $(1 - j)/\delta$, where δ is the skin depth in the metal. This forces the fields to decay with distance from the metal–insulator interface, in keeping with the skin effect. The fields discussed here are special cases of those presented in [3].

Continuity of E_z and H_x at the metal–insulator interface ($y = h_2$) requires that B and C in (1) and (2) satisfy

$$C = \cos(k_{\rm m}t_{\rm m}) \tag{5}$$

and

$$B = -\frac{k_{\rm i}}{\epsilon_{\rm i}}\,\frac{\epsilon_{\rm m}}{k_{\rm m}}\,\sin(k_{\rm m}t_{\rm m}). \tag{6}$$

Continuity of E_z and H_x at the insulator–semiconductor interface ($y = h_1 = t_{\rm s}$) yields two conditions for D that must be satisfied simultaneously. They are

$$D = \frac{B\,\sin(k_{\rm i}t_{\rm i}) + C\,\cos(k_{\rm i}t_{\rm i})}{\sin(k_{\rm s}t_{\rm s})} \tag{7}$$

and

$$D = \frac{k_{\rm s}}{\epsilon_{\rm s}}\,\frac{\epsilon_{\rm i}}{k_{\rm i}}\,\frac{C\,\sin(k_{\rm i}t_{\rm i}) - B\,\cos(k_{\rm i}t_{\rm i})}{\cos(k_{\rm s}t_{\rm s})}. \tag{8}$$

Since the modal propagation constant γ must allow (7) and (8) to be satisfied simultaneously, the fields of a mode may be found by altering γ until both (7) and (8) are satisfied simultaneously, at which point the modal fields of (1)–(3) will satisfy Maxwell's equations everywhere in the line. This procedure can be used to determine the fields and propagation constant of any of the TM modes of the MIS line.

The usual definitions for the modal voltage v_0 and the modal current i_0 per unit width are

$$v_0 \equiv -\int_{y=0}^{h_3} E_y\,dy \tag{9}$$

and

$$i_0 \equiv \oint \boldsymbol{H}\cdot dl = H_x|_{y=h_2} = \frac{j\omega\epsilon_{\rm m}}{k_{\rm m}}\,\sin(k_{\rm m}t_{\rm m}). \tag{10}$$

Here, the modal voltage v_0 corresponds to the integral of the tangential electric field across the transmission-line cross section from the electric wall at $y = 0$ and the magnetic wall at $y = h_3$. The modal current i_0 corresponds to the current in the metal film, determined here by integrating the magnetic field around a path enclosing the metal. The modal power p_0 per unit width, equal to the integral of the Poynting vector over y, is

$$p_0 = -\int_{y=0}^{h_3} E_y H_x^*\,dy. \tag{11}$$

In accordance with [4] and [5], the power–voltage definition of the characteristic impedance is $Z_0 \equiv |v_0|^2/p_0^*$ and the power–current definition of characteristic impedance is $Z_0 \equiv p_0/|i_0|^2$. We determine the inductance L, capacitance C, resistance R, and conductance G per unit length and width of the line from $R + j\omega L \equiv \gamma Z_0$ and $G + j\omega C \equiv \gamma/Z_0$. Figs. 3–5 plot exact solutions for these quantities for the current–power definition of Z_0 in solid lines for a substrate thickness $t_{\rm s} = 100$ μm. The figures illustrate the strong frequency dependence of L, C, R, and G.

III. Conventional Model

We will first investigate a simple equivalent-circuit model for the $\rm TM_0$ mode of the MIS line based on classic surface-impedance and parallel-plate-capacitor approximations. While this model cannot be found in the literature, it is composed of various elements of the models found in [1]–[3]. For this reason, we will call it the "conventional model."

Fig. 2 shows the model elements and their relationships to the standard parameters R, L, G, and C. The obvious analogy of the MIS line with a parallel-plate capacitor suggests setting $G_{\rm i} + j\omega C_{\rm i}$ and $G_{\rm s} + j\omega C_{\rm s}$ in the model of Fig. 2 to $j\omega\epsilon_{\rm i}/t_{\rm i}$ and $j\omega\epsilon_{\rm s}/t_{\rm s}$. The model reproduces the exact values of G and C on thin substrates extremely accurately.

However, the conventional model breaks down on thicker substrates. Figs. 3–5 illustrate this. They compare the exact

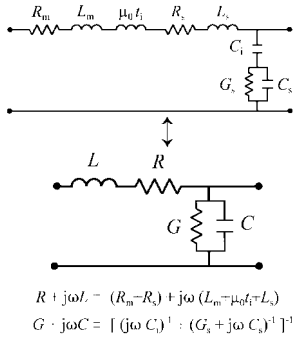

Fig. 2. An equivalent-circuit model for the TM_0 mode of the MIS transmission line of Fig. 1. The formulas at the bottom of the figure can be used to transform between the model parameters and the line's standard circuit parameters R, L, G, and C plotted in Figs. 3–5. The inductance attributed to the insulating region in the model is $\mu_0 t_\mathrm{i}$.

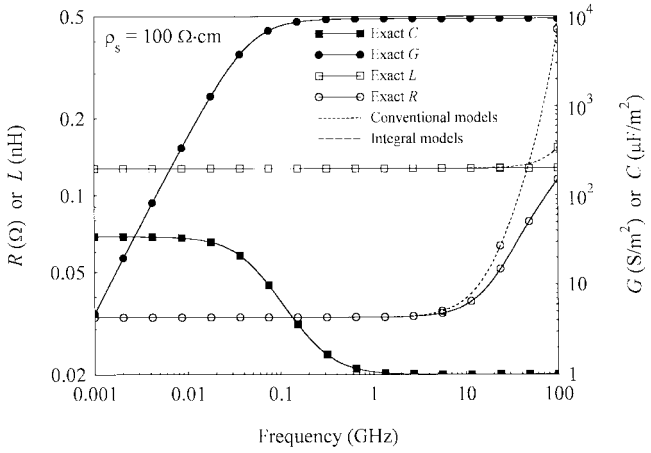

Fig. 3. Exact and modeled values of R, L, G, and C for the TM_0 mode of an MIS transmission line with $t_\mathrm{m} = t_\mathrm{i} = 1\ \mu$m, $\sigma_\mathrm{m} = 3 \times 10^7$ S/m, $\epsilon_\mathrm{i}' = 3.9$, $\epsilon_\mathrm{s}' = 11.7$, $\rho_\mathrm{s} = 100\ \Omega \cdot$ cm, and $t_\mathrm{s} = 100\ \mu$m. The integral model agrees so well with the exact results that the differences shown in the figure are indistinguishable. The exact values are calculated from the power–current definition of characteristic impedance.

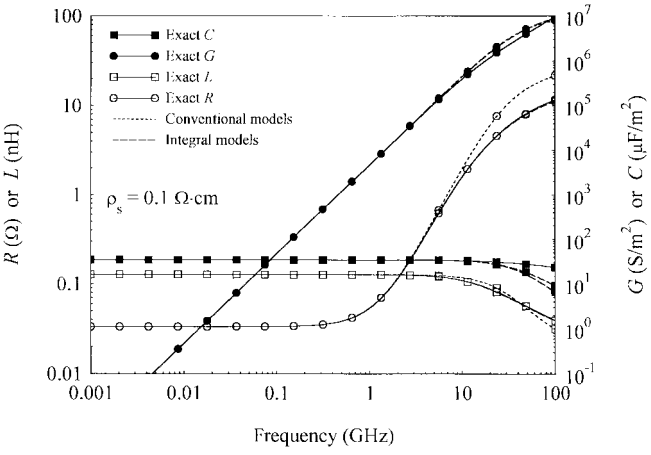

Fig. 4. Exact and modeled values of R, L, G, and C for the TM_0 mode of an MIS transmission line with $t_\mathrm{m} = t_\mathrm{i} = 1\ \mu$m, $\sigma_\mathrm{m} = 3 \times 10^7$ S/m, $\epsilon_\mathrm{i}' = 3.9$, $\epsilon_\mathrm{s}' = 11.7$, $\rho_\mathrm{s} = 0.1\ \Omega \cdot$ cm, and $t_\mathrm{s} = 100\ \mu$m. The integral model agrees so well with the exact results that the differences shown in the figure are, for the most part, indistinguishable. The exact values are calculated from the power–current definition of characteristic impedance.

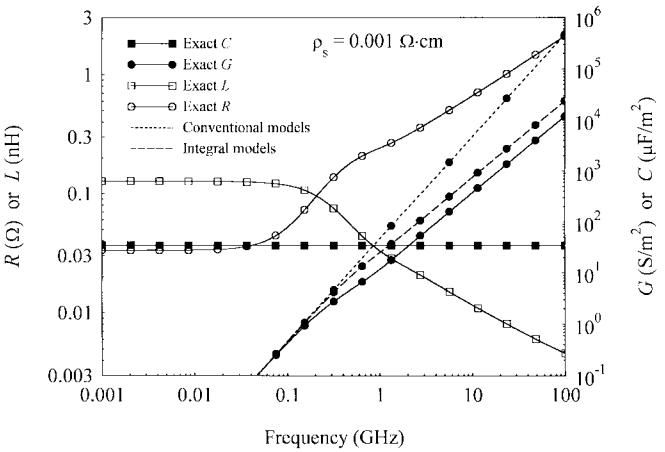

Fig. 5. Exact and modeled values of R, L, G, and C for the TM_0 mode of an MIS transmission line with $t_\mathrm{m} = t_\mathrm{i} = 1\ \mu$m, $\sigma_\mathrm{m} = 3 \times 10^7$ S/m, $\epsilon_\mathrm{i}' = 3.9$, $\epsilon_\mathrm{s}' = 11.7$, $\rho_\mathrm{s} = 0.001\ \Omega \cdot$ cm, and $t_\mathrm{s} = 100\ \mu$m. The models agree so well with the exact results that the differences shown in the figure are, for the most part, indistinguishable. The exact values are calculated from the power–current definition of characteristic impedance.

values of C and G for a 100-μm-thick substrate of various conductivities to those calculated from this model, which is labeled conventional model and marked with short dashed lines in the figures. Fig. 5 shows that the conventional model overestimates G significantly at high frequencies on thick highly conductive substrates.

The classic surface-impedance formulation approximates R_m and L_m by the surface impedance of a plane wave impinging on the finite metal film backed by a magnetic wall, and R_s and L_s by the surface impedance of a plane wave impinging on the finite thickness semiconducting substrate backed by a perfectly conducting ground plane. The resulting expression for R_m and L_m in the model of Fig. 2 is

$$R_\mathrm{m} + j\omega L_\mathrm{m} \approx \frac{jk_\mathrm{m1}}{\omega\epsilon_\mathrm{m}} \frac{1}{\tan(k_\mathrm{m1} t_\mathrm{m})} \tag{12}$$

and for R_s and L_s is

$$R_\mathrm{s} + j\omega L_\mathrm{s} \approx \frac{jk_\mathrm{s1}}{\omega\epsilon_\mathrm{s}} \tan(k_\mathrm{s1} t_\mathrm{s}) \tag{13}$$

where the $k_{\tau 1} \equiv \omega\sqrt{\mu_0\epsilon_\tau}$ [1]. These expressions may be derived by setting $\gamma = 0$ in (4) and substituting the resulting k into (1) and (2) to determine the surface impedances $-E_z/H_x$ at the metal and semiconductor surfaces.

The surface-impedance approximation, like its counterpart for C and G, works extremely well for thin substrates, but breaks down for thick substrates. This is illustrated in Figs. 3–5, which compare the exact values of R and L (solid lines) to those calculated from this surface-impedance approximation, which are also labeled conventional model and marked with short dashed lines. Fig. 3 shows that the conventional model overestimates R and L significantly at high frequencies on thick highly resistive substrates.

Thus, while the conventional model always gives good results for thin substrates, at high frequencies and on thick substrates, it overestimates G and C when the substrate conductivity is high and overestimates R and L when the

substrate conductivity is low. This is not surprising given that the approximations for G and C evolved from ideas based on insulting substrates and the approximations for R and L evolved from a surface impedance developed for good conductors.

IV. Volume Integral Expressions

While the approximations described above are good, we can do better with the new and exact integral expressions for R, L, G, and C found in [4] and [5]. For the TM modes of the one-dimensional MIS line, these integral equations reduce to

$$R + j\omega L = \frac{j\omega}{|i_0|^2} \int_{y=0}^{h3} (\mu_0 |H_x|^2 - \epsilon^* |E_z|^2)\, dy \tag{14}$$

and

$$G + j\omega C = \frac{j\omega}{|v_0|^2} \int_{y=0}^{h_3} \epsilon |E_y|^2\, dy. \tag{15}$$

While (14) and (15) are exact, we can develop good closed-form approximations by evaluating v_0, i_0, and the integrals only in the semiconducting substrate. Thus, we substitute the integration limit h_1 at the silicon surface for h_3, H_x at the semiconductor surface ($y = h_1 = t_s$) for i_0 in (14), $-\int_{y=0}^{h_1} E_y\, dy$ for v_0 in (15), and k_{s2} for k_s, where

$$k_{s2}^2 \equiv \omega^2 \mu_0 \epsilon_s + j\omega \frac{(\sigma_m t_m)^{-1} + j\omega\mu_0(t_i + t_m)}{t_i/\epsilon_i + t_s/\epsilon_s}. \tag{16}$$

The expression for k_{s2} comes from substituting γ derived from approximate equivalent-circuit parameters into (4) evaluated in the silicon substrate. This results in the approximations

$$\begin{aligned} R_s + j\omega L_s \approx{}& \frac{j\omega}{2|\cos(k_{s2}t_s)|^2} \\ &\cdot \left[\mu_0 \left(\frac{\sin(2k'_{s2}t_s)}{2k'_{s2}} + \frac{\sinh(2k''_{s2}t_s)}{2k''_{s2}} \right) \right. \\ &\left. + \left| \epsilon^* \frac{k_{s2}}{\omega\epsilon_s} \right|^2 \left(\frac{\sin(2k'_{s2}t_s)}{2k'_{s2}} - \frac{\sinh(2k''_{s2}t_s)}{2k''_{s2}} \right) \right] \end{aligned} \tag{17}$$

and

$$\begin{aligned} G_s + j\omega C_s &\approx \frac{j\omega\epsilon_s |k_{s2}|^2}{2|\sin(k_{s2}t_s)|^2} \left(\frac{\sin(2k'_{s2}t_s)}{2k'_{s2}} + \frac{\sinh(2k''_{s2}t_s)}{2k''_{s2}} \right) \end{aligned} \tag{18}$$

where k'_{s2} and k''_{s2} are the real and imaginary parts of k_{s2}. Figs. 3–5 plot the results of this approximation with long dashed lines and label them "integral models." These volume integral models are so good that they usually cannot be distinguished from the exact results on the figures, although Fig. 5 shows that (18) overestimates G somewhat on thick highly conductive substrates at high frequencies.

V. High-Loss Region of Operation

Up to this point we have examined only the TM_0 mode. When the substrate is thin, the loss of the TM_0 mode is always small compared to those of the higher order modes of propagation, and it can be considered to be "dominant." That is to say, its loss is so low that all higher order modes created at a discontinuity in the line die away quickly enough to be ignored at small distances from the discontinuity. When the TM_0 mode is dominant, it is the only mode that carries power between well separated sources, discontinuities, and receivers in the line.

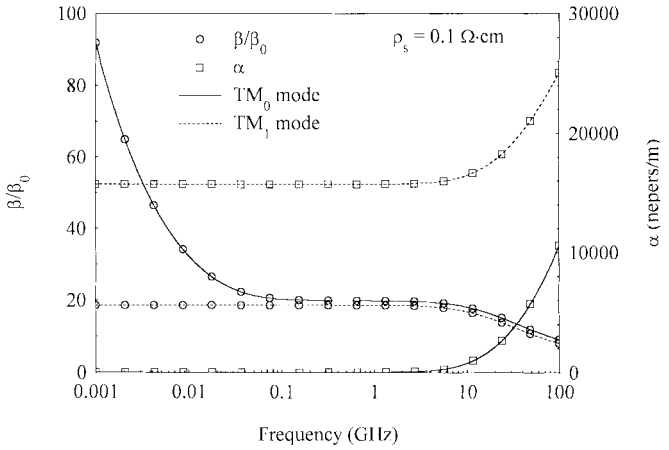

Fig. 6. The attenuation constant α and normalized phase constant β/β_0 of the TM_0 and TM_1 modes at $\rho_s = 0.1\ \Omega \cdot$ cm for an MIS transmission line with $t_m = t_i = 1\ \mu$m, $\sigma_m = 3 \times 10^7$ S/m, $\epsilon'_i = 3.9$, $\epsilon'_s = 11.7$, and $t_s = 100\ \mu$m. The quantities α and β are defined from $\gamma \equiv \alpha + j\beta$ and β_0 is the phase constant of a plane wave propagating in free space.

The exact method can be used to find the propagation constant and fields of any TM_n mode. Fig. 6 plots the attenuation constants α of the TM_0 and TM_1 modes as a function of frequency when $\rho_s = 0.1\ \Omega \cdot$ cm for a substrate thickness of $t_s = 100\ \mu$m. The figure shows that at low frequencies, the attenuation of the TM_0 mode remains small compared to that of the TM_1 mode. At these frequencies, the TM_0 is dominant, has fairly low attenuation, and is thus well suited for propagating electrical signals.

However, the attenuation constant of the TM_0 modes grows rapidly at high frequencies, making it poorly suited for propagating high-frequency signals. Figs. 7 and 8 show that this high-loss region is limited to high frequencies and a limited band of substrate resistivities near $\rho_s = 0.1\ \Omega \cdot$ cm.

Fig. 6 shows that in its high-loss region of propagation, the attenuation constant of the TM_0 mode becomes comparable to that of the TM_1 mode. Here, we can no longer say that the TM_0 mode is dominant and an accurate description of the line will require consideration of multiple modes of propagation, a considerable design complication. There are other design complications in this high-loss region as well.

Figs. 7 and 8 plot $\zeta_{01} \equiv |p_{01}p_{10}/p_{00}p_{11}|$, a measure of the significance of the modal cross powers [7], where

$$p_{nm} \equiv -\int_{y=0}^{h_3} E_{yn} H^*_{xm}\, dy \tag{19}$$

and E_{yn} and H_{xn} are the fields of the TM_n mode. They show that ζ_{01} becomes large when the propagation constants of the two modes become comparable. When ζ_{01} is large, the total power in the transmission line can no longer be calculated as a sum of the powers carried individually by the TM_0 and TM_1 modes [8]. This emphasizes the complexity and multimodal

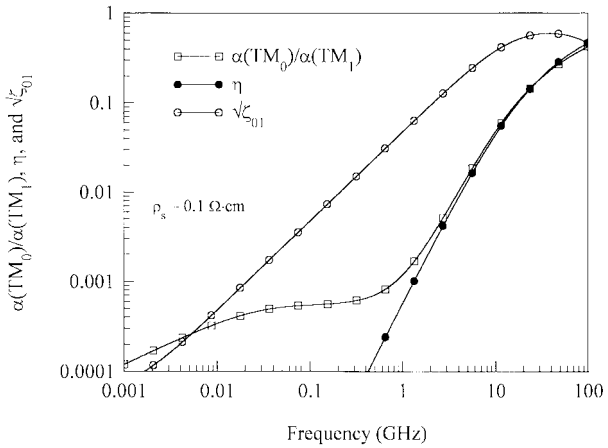

Fig. 7. The ratio of attenuation constants of the TM_0 and TM_1 modes, η, and ς_{01} at $\rho_s = 0.1\ \Omega \cdot$ cm for an MIS transmission line with $t_m = t_i = 1\ \mu$m, $\sigma_m = 3 \times 10^7$ S/m, $\epsilon_i' = 3.9$, $\epsilon_s' = 11.7$, and $t_s = 100\ \mu$m.

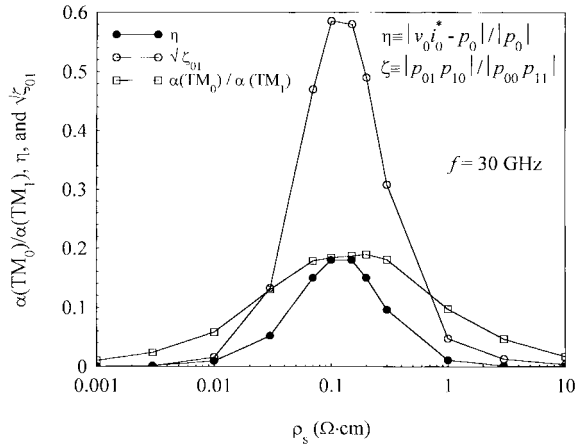

Fig. 8. The ratio of attenuation constants of the TM_0 and TM_1 modes, η, and ς_{01} at 30 GHz for an MIS transmission line with $t_m = t_i = 1\ \mu$m, $\sigma_m = 3 \times 10^7$ S/m, $\epsilon_i' = 3.9$, $\epsilon_s' = 11.7$, and $t_s = 100\ \mu$m.

character of the transmission line in its high-loss region of operation.

Figs. 7 and 8 also plot $\eta \equiv |v_0 i_0^* - p_0|/|p_0|$, a measure of the fidelity with which the power carried by the TM_0 mode is determined by the product $v_0 i_0^*$ of its modal voltage and the conjugate of its modal current. The figures show that the usual relationship between the conventionally defined modal voltage and current and the actual power carried in the line fails in the high-loss region.

MIS lines with high-loss regions of operation may be used to propagate low-frequency signals over moderate distances and high-frequency signals over very short distances. However, even though the integral-based equivalent-circuit model still provides an accurate description of the propagation characteristics of the TM_0 mode in its high-loss region, the preceding discussion paints a complex picture of the electromagnetic behavior of the MIS line there. Accurate high-frequency circuit design in this high-loss region will require accounting for the multimodal character of the transmission line, high modal cross powers, and unconventional relationships between the modal voltage, current, and power.

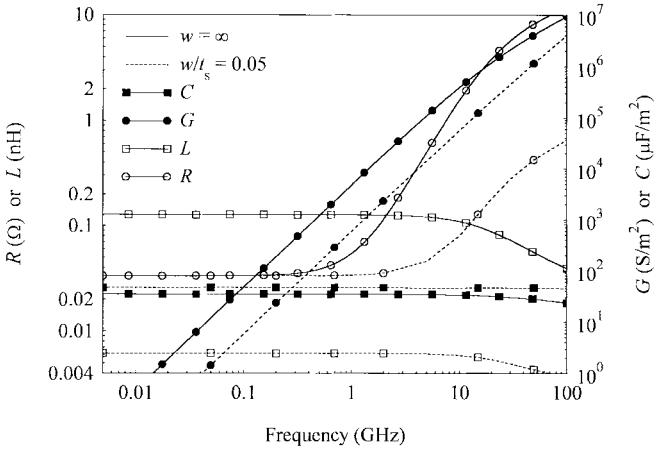

Fig. 9. Exact values of R, L, G, and C for the TM_0 mode of the one-dimensional MIS transmission line with $t_m = t_i = 1\ \mu$m, $\sigma_m = 3 \times 10^7$ S/m, $\epsilon_i' = 3.9$, $\epsilon_s' = 11.7$, $\rho_s = 0.1\ \Omega \cdot$ cm, and $t_s = 100\ \mu$m are compared to results for microstrip calculated with the full-wave method of [9]. The parameter w is the width of the microstrip center conductor and the case $w = \infty$ refers to the one-dimensional results.

VI. Microstrip

While we made no attempt to account for the fringing fields of a finite-width microstrip in the one-dimensional analysis presented here, it is reasonable to ask whether the one-dimensional MIS line will provide an accurate model for a finite-width microstrip line. In fact, the model works well for w larger than t_s. Calculations show, for example, that wider microstrip reflects the qualitative behavior of the one-dimensional MIS line and still exhibit, for example, a high-loss region near $\rho_s = 0.1\ \Omega \cdot$ cm.

However, the one-dimensional model breaks down when w becomes much smaller than t_s. This breakdown is illustrated by Fig. 9, which compares the equivalent-circuit parameters of a microstrip line of center conductor widths $w = 0.05 t_s$ determined with the full-wave method of [9] to those of the one-dimensional MIS line. Here, the equivalent-circuit parameters of the microstrip line has been normalized by w, so as to be directly comparable to the one-dimensional results. That is, R and L for the microstrip line has been multiplied by w, whereas G and C have been divided by w. In each case, the metal, insulator, and substrate parameters were all identical.

Fig. 9 shows that the fringing fields cannot be ignored when w is much smaller than t_s and the one-dimensional MIS results cannot be used for practical circuit design. It indicates, for example, that the microstrip-line inductance L cannot be predicted by simply dividing the inductance of the one-dimensional MIS line by the conductor width w. The figure also shows that the effect of the substrate on R weakens as the center conductor width shrinks, suggesting that narrow microstrips on silicon substrates may avoid the high-loss region of operation discussed above.

VII. Conclusion

This paper presented accurate closed-form models for the equivalent-circuit parameters of the TM_0 mode of the one-dimensional MIS transmission line. In contrast to previous treatments, only a single set of expressions and model topol-

ogy are required to describe the line over its entire range of operating conditions. This simplification creates a clear physical picture of the MIS line, in which the impedances and admittances of each layer may be calculated independently and then added together in a simple and intuitive way to predict overall transmission-line behavior. In this picture, the series impedance of each layer is determined by its surface impedance and its admittance by a parallel-plate capacitance model.

The accuracy of the conventional model was improved with the aid of the integral expressions of [4] and [5]. This improvement did not require adding elements to the model or adjusting the model topology. This is the first time, to the author's knowledge, that these integral equations have been used to estimate equivalent-circuit parameters. The success of this approach here suggests a new methodology for constructing equivalent circuits for more complex transmission lines. This methodology would use field approximations and the integral expressions of [4] and [5] to estimate the contributions of each layer or physical region of the transmission line to the total transmission-line impedance and admittance per unit length.

This paper has also shown that the MIS line has a high-loss region of operation in which its electrical behavior becomes complicated and multimodal in nature. It explored the properties of the TM_0 mode in this high-loss region of operation, showing that the conventional relationships between its modal voltage, current, and power do not hold there, and that the total power in the line is no longer a simple sum of the powers carried by each mode of propagation individually. From this last observation, we can conclude that accurate treatments of MIS lines in this high-loss region will require consideration not only of multiple modes of operation, but also of the modal cross powers, as is done in [8].

ACKNOWLEDGMENT

The author would like to thank U. Arz and D. DeGroot for sharing their many useful insights concerning the physics of the MIS transmission line.

REFERENCES

[1] H. Guckel, P. A. Brennan, and I. Palócz, "A parallel-plate waveguide approach to microminiaturized, planar transmission lines for integrated circuits," *IEEE Trans. Microwave Theory Tech.*, vol. MTT-15, pp. 468–476, Aug. 1967.

[2] H. Hasegawa, M. Furukawa, and H. Yanai, "Properties of microstrip line on $SiSiO_2$ system," *IEEE Trans. Microwave Theory Tech.*, vol. MTT-19, pp. 869–881, Nov. 1971.

[3] D. Jäger, "Slow-wave propagation along variable Schottky-contact microstrip line," *IEEE Trans. Microwave Theory Tech.*, vol. MTT-24, pp. 566–573, Sept. 1976.

[4] R. B. Marks and D. F. Williams, "A general waveguide theory," *J. Res. Natl. Bur. Stand.*, vol. 97, no. 5, pp. 533–562, Sept./Oct. 1992.

[5] J. R. Brews, "Transmission line models for lossy waveguide interconnections in VLSI," *IEEE Trans. Electron Devices*, vol. ED-33, pp. 1356–1365, Sept. 1986.

[6] R. E. Collins, *Field Theory of Guided Waves.* New York: McGraw-Hill, 1960.

[7] D. F. Williams and F. Olyslager, "Modal cross power in quasi-TEM transmission lines," *IEEE Microwave Guided Wave Lett.*, vol. 6, pp. 413–415, Nov. 1996.

[8] D. F. Williams, L. A. Hayden, and R. B. Marks, "A complete multimode equivalent-circuit theory for electrical design," *J. Res. Natl. Bur. Stand.*, vol. 102, no. 4, July/Aug. 1997.

[9] W. Heinrich, "Full-wave analysis of conductor losses on MMIC transmission lines," *IEEE Trans. Microwave Theory Tech.*, vol. 38, pp. 1468–1472, Oct. 1990.

Dylan F. Williams (S'82–M'86–SM'90) received the Ph.D. degree in electrical engineering from the University of California at Berkeley, in 1986.

In 1989, he joined the Electromagnetic Fields Division, National Institute of Standards and Technology, Boulder, CO, where he develops metrology for the characterization of monolithic microwave integrated circuits and electronic interconnects. He has published over 60 technical papers.

Dr. Williams was the recipient of the Department of Commerce Bronze and Silver Medals, the Electrical Engineering Laboratory's Outstanding Paper Award, two ARFTG Best Paper Awards, the ARFTG Automated Measurements Technology Award, and the IEEE Morris E. Leeds Award.